The state of the atmosphere throughout the seasons: how well can atmospheric models explain infrasound observations at regional distances

Karl Koch, Christoph Pilger

Federal Institute for Geosciences and Natural Resources

Stilleweg 2

D-30655 Hannover

Abstract

Over the past two decades the German Aerospace Center facility near Heilbronn, Germany, has conducted a considerable number of tests of the ARIANE-5 main rocket engine. From the 159 studied tests a large portion (~45%) was detected at IMS infrasound station IS26 in the Bavarian forest, located at a distance of about 320 km in an eastward direction (99° clockwise from North). Observations were mostly made during the winter season between October and April with a detection rate of more than 70%, as stratospheric winds then favour atmospheric infrasound propagation within a stratospheric duct. For the summer season the reversal of middle atmospheric wind patterns generally inhibits signal detections, as is found by comparisons of numerical weather prediction models. A significant portion of non-detection cases during winter, however, also exhibit a sound speed profile that should enable infrasound signal observations due to the presence of a stratospheric duct. Using European Centre for Medium-Range Weather Forecast (ECMWF) atmospheric model analysis and infrasound propagation modelling it was found that about two-thirds can be explained by the existence of a shadow zone near the station. For one third of the cases, however, such a shadow zone does not exist and it must be concluded that the applied atmospheric model is more often than expected unable to correctly explain infrasound propagation to regional distances, as has been found in previous studies.

Keywords: infrasound, atmospheric models, ground truth source, stratospheric ducting, regional distances, rocket engine tests

1. Introduction

Infrasound signals in the atmosphere from natural and anthropogenic events propagate in a very dynamic and anisotropic medium. Compared to the propagation of seismic waves, the solid earth can be considered a static medium. With the dawn of the Comprehensive Nuclear-Test-Ban Treaty (CTBT), incepted in 1996 after decade-long disarmament negotiations for the monitoring of all environments towards banning nuclear explosion test explosions, the infrasound technology has experienced a rebirth to the research activities in the 1950s and 1960s.Then, atmospheric testing was extensively carried out, but was banned by the LTBT (Limited Test Ban Treaty) in 1963, prohibiting nuclear testing in outer space, under water and in the atmosphere (Dahlman et al, 2010).

Numerous studies in recent years (c.f. Le Pichon et al, 2008; Koch, 2010; Green et al., 2011; Fuchs et al., 2019; Koch & Pilger, 2019; Koch & Pilger, 2020) have found examples that the atmospheric specification available from analysis data of numerical weather prediction(NWP) models may not necessarily describe infrasound observations at regional distances adequately enough. In these cases numerical propagation calculations were not always able to predict the observed arrivals, in that the atmospheric models do not include the corresponding duct that is most likely implied to exist based on the wave field parameters extracted from the recorded signals. As initially described by Le Pichon et al. (2008) or Koch (2010) infrasound detection throughout Central Europe is governed by the seasonal switch of the stratospheric wind pattern near the spring and fall equinoxes, with the stratospheric wind pattern pointing towards the east during winter months and reversing during the summer. This consistent pattern has been demonstrated to exist by Koch (2010) who has studied infrasound observations from rocket engine tests carried out for the ARIANE-5 main booster engine for development tests carried out between the years 2000-2004, at a distance of about 300 km at IMS station IS26 to the east-southeast from the source site. In this period infrasound signals from these tests were only observed in the months from November to April, whereas no observations were made during the rest of the year. This observation was further made during a field campaign from late 2011 to May 2012 (Pilger et al.,2013).However, during the campaign we also made an infrasound observation in May 2012, where ray tracing with the European Centre for Medium-Range Weather Forecast (ECMWF) model did not produce an arrival at IS26, except when introducing model variations from gravity wave perturbations (Gardner et al., 1993).

In fall of 2018 (3 September) an explosion near Ingolstadt, Southern Germany, provided an impressive number of infrasound observations within a few hundred kilometers providing clear evidence that standard NWP models may fail in specific cases to model infrasound arrivals(Fuchs et al., 2019; Koch & Pilger, 2020). In these cases the model provided strong evidence of sole (or multipathed) thermospheric returns at distances between 200 and 600 km distances, while results from waveform

analyses provide strong indications that the observed arrivals were indeed from stratospheric ducting based on obtained estimates of celerity and trace velocity.

Other studies (Le Pichon et al., 2015; Hupe et al., 2019) have been conducted in the framework of the Atmospheric Dynamics Research Infrastructure in Europe (ARISE) project (Blanc et al., 2018) and were aimed at assessing the accuracy of middle atmosphere numerical weather prediction models, e.g., from ECMWF. In these studies model data from ECMWF were compared to estimates of temperature and wind speed components from satellite and ground based observation systems. Le Pichon et al. (2015) found from lidar and wind radiometer measurements at the OHP observatory that results are broadly consistent with the ECMWF model for altitudes up to ~40 km, but differences become significant for greater heights, with differences exceeding 5°K for temperature and 20m/s for zonal wind. Hupe et al (2019) investigated the temperature field of ECMWF models with the temperature field from Compact Rayleigh Autonomous Lidar measurements which indicated a cold bias above 40 km with a maximum near 60 km altitude of about 12K, with two standard deviations of 4.5-6°K. They also evaluated the impact on the detection pattern for microbaroms after inclusion of uncertainties in temperature and horizontal winds and found a significant improvement compared to the direct output of the ECMWF model.

Since the German Aerospace Center (Deutsches Zentrum für Luft- und Raumfahrt/DLR) facility near Heilbronn, Germany, has conducted a considerable number of tests of the ARIANE-5 main engine over the past two decades, we take here the opportunity of a large ground-truth dataset of about 160 rocket engine tests to investigate the adequacy of the ECMWF models in correctly predicting arrivals or non-arrivals at station IS26 in the Bavarian Forest (see also Figure 1). In particular we focus on those cases where we lack an observation when an arrival is predicted, and on other cases when arrivals exist but the model fails to predict them. The distance range of 300 km is of particular interest since it normally partitions the range of tropospheric wave propagation from the range where atmospheric infrasound starts to show stratospheric ducting, with both ranges being separated by an acoustic shadow zone (Gutenberg, 1939). As to how prominent this shadow zone impacts on non-detections will further be studied.

As detailed below, this study is significantly different in scope from the recent study by Pilger et al. (2021), where the infrasonic signature of 1001 rocket launches, including 66 ARIANE-5 rockets, wereinvestigated. While long-range infrasound detectability of this type of rocket was clearly proven there, the present study aims primarily at regional infrasound propagation and at a different ARIANE 5 source configuration. Firstly, we study here infrasound emitted from the main engine, while in the previous study additional booster stages are involved. And secondly, we deal in this study with a

spatially fixed ground-truth source, while Pilger et al. consider a laterally and vertically moving infrasound source along its flight path.

2. The ground-truth source and its location from the receiver

The ground truth source being used for this study is the one already described by Koch (2010), and which was further the subject of Pilger et al.'s (2013) study. In the 1990s, the Space Propulsion Institute of DLR at Lampoldshausen near Heilbronn, Southern Germany, established a testing facility (called P5) within the development programme for the ARIANE-5 main engine. This facility is located at latitude 49.3°N and longitude 9.4°E (Figure 1). While in the early years, up to 2004, the purpose of the facility was testing of the design concepts for the VULCAIN I and II engines, the testing later shifted to acceptance testing before use in the space flight programme of the European Space Agency (ESA), which has continued to the present. For each test the main engine of ARIANE-5 with a thrust of 1000 kN is mounted in the P5 facility and, hence, provides fairly identical setups for each test, including the deflection of the propulsion jet towards the southeast, approximately in the direction to the infrasound array station IS26 recording the atmospheric pressure waves. Therefore we assume that the infrasound generation mechanism is nearly identical from test to test and that regional infrasound observations are, for the most part, governed by the atmospheric parameters at the times of the tests.

As shown in Figure 1, IMS station IS26 is located at an azimuth of ~100° and a distance of ~320 km from Lampoldshausen. With known test duration and the theoretical backazimuth of 282°, two parameters are available to reliably identify the infrasound signal in the observations: (1) the signal duration in the waveforms and (2) the backazimuth from array processing techniques are to be matched when declaring detection. From 2000 to 2019 we received the ground-truth parameters (date & time, test duration) for more than 170 engine tests by DLR, of which about a dozen had durations of less than 10 seconds, while nearly 100 tests lasted more than 600 seconds (10 mins), being considered the minimum thrusting time of this stage for a successful rocket launch. From all tests, nearly 100 were carried out during the initial five years starting in 2000 (Koch, 2010), whereas for another set of more than 70 tests over the subsequent 15 years the ground-truth information was collected recently (K. Fröhlke, pers. communication). Only for one test the corresponding waveform data could not be found in our data archive.

3. Data analysis

With the distance of 320 km between IS26 and Lampoldshausen and celerities of tropospheric acoustic waves of 320-350 m/s (Negraru et al., 2010), such waves would arrive between 15 and 16 min after the propulsion test's origin time, while stratospheric waves with celerities of 280-320 m/s would arrive another 2mins later. Within these delay time windows an interactive search for corresponding signal onsets was carried out. When the signal could be identified, mainly based on the signal duration corresponding to the propulsion duration, a frequency-wavenumber (F-K) analysis (Stammler, 1993) was carried out to find the backazimuth and the apparent velocity (or slowness). In most cases a signal could be identified, reflecting the theoretical backzimuth within a few degrees.

In Figure 2 the waveforms are shown for a couple of events that were detected at IS26 with different signal to noise ratios (SNR). The data are filtered with a high-pass filter of 2 Hz. The frequency range considered in this study is therefore beyond the frequency band commonly considered in infrasound studies based on IMS stations, ranging between a few seconds period and several Hz (Campus, 2004; Campus & Christie, 2010). The waveforms of the upper two events, where signals above 3 Hz clearly stand out from the background noise, represent data with a rather decent SNR of about 3 to 5. The third event shows more emergent, and hence less prominent, waveforms with a SNR of between 1 and 2. The lower waveforms are from two events that do not exhibit any engine test signals, but only noise bursts or signals of no interest. One case is from a propulsion test in winter (Dec 2000), where atmospheric ducting conditions between the DLR facility and IS26 are usually favourable; while for the second case of a test in summer (July 2001) the propagation conditions normally do not allow the observation of a signal.

As previously found for Central Europe, pressure sources west of infrasound stations lead to frequent infrasound detections from fall to spring equinoxes, while signal detections are prominent from the opposite direction during summer months (Le Pichon et al., 2008; Koch, 2010;Green et al., 2011; Gibbons et al., 2015; Pilger et al., 2018). Figure 3 as well as Table 1 summarize the detection statistics for all 159 ARIANE engine tests from 2000 to 2019 as observed at IS26, and hence follow this pattern. In this compilation all tests of duration less than 10 sec were left out, as they may not have been easily identified due to the short duration or an inability to obtain stable F-K analysis results. Except for a single observation each in May and September all other 69 tests yielding infrasound signals occurred only from October to April, where a majority of all conducted engine tests could be detected; only one quarter of the tests in these winter months resulted in non-detections at IS26.Non-detections in the summer months May to September are pervading, i.e. for 63 (97%) out of 65 engine tests in the summer season it was not possible to find an associated signal.

For each identified infrasound signal a frequency-wavenumber analysis was carried out. The raw waveform data were high-pass filtered with 2 or 3 Hz, depending on the optimal signal, and a frequency wavenumber analysis was carried out for frequencies up to 6 Hz. A maximum slowness range of 450 s/deg was applied with a discretization of 120 points, as required by the analysis program (Stammler, 1993), covering trace velocities down to 250 m/s. The associated results gathered for backazimuth, slowness and apparent velocity are displayed in Figure 4. The theoretical backazimuth from IS26 to Lampoldshausen is well represented with azimuths scattering with about 5-6 ° with respect to the expected value of 282°. For slowness we obtained mostly values between 300-340 s/deg, translating into trace velocities between 330 and 370 m/s. These values indicate therefore stratospheric ducting, as they appear to exceed the near surface sound velocities of 330-340 m/s. In Figure 4 a stronger scatter in the estimated array processing results seems to occur prior to 2008 which may be related to the upgrade from a five-element to an eight-element infrasound array, providing more stable array processing results.

In order to assess the fraction of non-detections that may be due to increased background noise levels at the IS26 array we present signal vs. noise levels for detections and only noise levels for the cases of non-detections from element I26H1, as shown in Figure 5. For identified signals the estimation was carried out in windows being representative. They were set such to include, if possible, the entire signal, but in the presence of spikes or noise bursts to exclude them. Noise signal estimates were made immediately preceding the signal window. In the case of non-detections the amplitude window was selected within the expected arrival time window. As signal and noise level measure the root-mean-squares (RMS) amplitude was taken, considered a stable amplitude estimate in the presence of incidental noise, such as spikes or bursts. First it is noted that noise levels prior to 2005 are somewhat higher than for later years, probably by some 50%. This effect should be associated with the noise reduction filter system at IS26, which was upgraded with impedance filters attached to the pipe outlets during 2004. In Koch (2010) signal levels at all elements of IS26 were assessed for the years 2000-2004 with a decrease found for I26H4 in 2003 when this element was equipped temporarily with such impedance reducers in a test to suppress spurious spectral peaks caused by the spatial noise reduction system used at IS26.

While noise levels are mostly below 0.015 amplitude units prior to 2005, the noise levels after 2004 are below 0.01 amplitude units. From this result, we conclude that non-detections with noise levels above this baseline level may not be found due to an insufficient signal-to-noise ratio. Of course, the opposite conjecture may also hold: events with pre-event signal levels (i.e. noise) below the baseline should be detected.

4. Numerical weather prediction models

As is well known (LePichon et al., 2015) atmospheric conditions are significantly different between spring and fall equinoxes, in particular with respect to the reversal of the dominant stratospheric wind direction. The particular atmospheric models considered here are based on the ECMWF atmospheric specification for altitudes up to 60-70 km which is then extended to greater heights by smooth transition to the climatological models HWM14 and MSISE00 (Drob et al., 2015; Picone et al., 2002). From the ECMWF models the six-hour analysis data were used including the physical parameters pressure, temperature and wind speeds. The model reference is established as a 1-D effective sound speed model at the midpoint between source (DLR) and receiver (IS26), geographically lying near the center of a triangle outlined by the cities of Nuremberg, Regensburg and Ingolstadt, while for the raytracing modeling we apply a 2D atmospheric model along the source receiver path.

The resulting models applicable for each ARIANE-5 engine test in the last 20 years for the cases with signal detections and cases with non-detections are examined and compared for gross specific features to explain the differences in observations (Figure 6). The 1D reference model is considered a good characterization of the atmospheric state, as the west-to-east conditions are quite stable over the distance range of 300km between source and receiver. All ECMWF reference models for the detection cases (Figure 6a) show a distinct maximum in effective sound speed leading to a strong stratospheric duct for altitudes between 40 and 60 km. This similarity of the atmospheric models is clearly reflected in the mean model and median model, which are closely matching. It further finds its expression in the standard deviation curves yielding an effective sound speed ratio, i.e. the ratio of the effective sound speed at stratospheric heights to the one near the ground, being above a value of 1, which, according to Le Pichon et al. (2012) represents a sufficient condition for stratospheric ducting. The ECMWF models for the non-detection cases (Figure 6b) show a contrasting picture, with most models not showing an effective sound-speed peak for stratospheric heights, therefore not enabling stratospheric ducting. This is, of course, reflected in the mean and median models which do not reach effective sound speed ratios of 1 and therefore explain well the non-observations. However, it is also shown that a considerable portion of atmospheric models for the cases of non-detections indicate the presence of a stratospheric duct with the potential for stratospheric arrivals; this dissimilarity with the majority of background models is therefore reflected in the clear mismatch between the mean and median models and the positive standard deviation curve. This latter curve also exhibits a sound speed ratio of larger than 1.

In Figures 7 histograms of the resulting effective sound speed ratios ($v_{eff\text{-}ratio}$) from the ECMWF model applying for infrasound detections and non-detections at the times of ARIANE-5 tests are displayed. The quantity shown is defined here as the ratio of the maximum effective sound speed in the altitude

range of 30 to 70 km to the maximum sound speed in the lower 5 km above the ground. For the 71 detections (Fig.7a) all but four showed ratios above 1, with the remaining ones falling short of this value by less than 1.5%. For the non-detections (Fig.7b) about one quarter of cases (20) shows effective sound speed ratios exceeding the enabling value of 1. These cases therefore deserve further discussion below.

Additional examination of the effective sound speed ratios over the seasons (Fig.8) in relation to allowed detections or not reveals an interesting, even though expected, pattern for winter and summer months (Le Pichon et al., 2008; Koch, 2010). Near the times of the equinoxes the $v_{eff\text{-}ratio}$ changes from values above 1 to values below 0.9. The most striking part is in particular the rather small scatter in the considered quantity during the summer, while the scatter can be on the order of 40-50% during the winter. In other words, the rather low variability of the effective sound speed ratios in the summer season explains the consistent lack of detections during this time. As effective sound speed is dominated by temperature and wind speeds, the strong scatter during winter is an expression of a higher variability of these parameters during winter between near-ground troposphere and middle atmosphere (stratosphere).

To further investigate the probability of signal detection for high $v_{eff\text{-}ratio}$ and to identify an underlying pattern Table 2 list the numbers of detections and non-detections depending on the $v_{eff\text{-}ratio}$ ordered in various ranges, namely >1.2, 1.1-1.2, 1.0-1.1, 0.98-1.0, and <0.98. The last class does not contain any detection, as is also indicated in Figs.7 and 8. In this table we give three different quality levels for the detections in terms of their signal strength and variability: (2) good, (1) weak, and (0) poor where good signal conditions indicate a SNR above 2-3 and weak and poor conditions those below 2; poor signals furthermore show instable signal content. In each column of the table we give two numbers depending on whether the atmospheric model shows a shadow zone or not, i.e., when a stratospheric duct can be expected to exist (for $v_{eff\text{-}ratio}$>1 or >0.98 when counting on gravity wave influences, respectively; see e.g. Pilger et al.,2013). Of the 36 cases with highest $v_{eff\text{-}ratio}$, i.e. >1.2, the overwhelming number of cases (~70%) consist of clear detections, with a few cases of weaker signals including very few cases of shadow zones, but also 5 cases (14%) of non-detections where only in one case a shadow zone is predicted for IS26, i.e. the range of about 320 km. For the next two categories of smaller $v_{eff\text{-}ratio}$, but still above 1, the number of detections with good signals decreases rapidly, but is somewhat compensated by detections with lesser signal levels, while the non-detections reach proportions of about 30%. In most of these cases the atmospheric model produces a shadow zone explaining well the absence of signals.

With the 25 detections for which the ECMWF and propagation modeling unambiguously predicts shadow zones and the 7 non-detections without an associated shadow zone (see Table2), we then find

32 cases of ARIANE tests that are not adequately dealt with by the atmospheric modeling in terms of the signal prediction by stratospherically ducted waves. A similar case has been seen for the Ingolstadt explosion, where both Fuchs et al. (2019) and Koch & Pilger (2020) identified clear stratospheric arrivals in cases where the ECMWF model was not able to produce them. Both studies therefore suggest that failure to predict stratospheric arrivals at regional distances is absolutely not a rare case, but can occur on the order of 20 percent of the cases. Of course, some of the cases with IS26 being actually or possibly within a stratospheric shadow zone could be treated within the framework of dynamic gravity wave coupling (Gardner et al.,1993). Such modification explains well the occurrence of a detection for the test on 14 May 2012, where the ECMWF model alone predicts a shadow zone, as studied by Pilger et al. (2013).

For quantifying the rate of the ECMWF model potentially failing to predict a signal detection at IS26 from the ARIANE tests, we can consider the 46 correctly predicted arrivals from propagation modeling with the 25 detections without success (see Table 2); hence, we get approximately a 1:2 chance of not being able to predict the correct propagation result.

For the case for $0.98 < v_{eff\text{-}ratio} < 1$, where we are relatively close to the case of stratospheric ducting, we obtain a surprisingly similar result when a 4:9 chance of detection versus non-detection is found. And finally we have the case of 20 non-detections (i.e. for $v_{eff\text{-}ratio} > 1$, see also Table3), of which 13 are explained by shadow zones, but 7 are not. Again we have a 1:2 chance of not explaining an observation correctly.

5. Investigations on cases of interest

Of specific interest in the interpretation of infrasound from the ARIANE-5 rocket engine tests are the cases where the $v_{eff\text{-}ratio}$ enables a stratospheric duct in general, but when a receiver can still not detect a stratospheric arrival. In this scenario we presume that the stratosphere is equally transparent to atmospheric waves over a larger frequency range, which is mostly the case (Sutherland & Bass, 2004, Waxler et al., 2017a). Often such scenarios then arise when the atmospheric models are such that the range and location of associated shadows zones (or zones of silence; Gutenberg, 1939) varies largely and is particularly pronounced at regional distance, so that detections or non-detections may occur on a case by case basis at a specific range like the 320 km distance studied here.

As has been found (see Table 2) there are 20 cases of ARIANE tests(see Table 3for a list of these cases), where no signal could be identified in the IS26 waveform data, even though stratospheric ducting follows from the $v_{eff\text{-}ratio} > 1$. While 13 of these tests are associated with a shadow zone according to the

ECMWF model, the remaining 7 tests do not exhibit such a zone; thus signals are expected to occur, as is demonstrated in Figure 9. The propagation modeling has been carried out with a 2D raytracing code (Margrave and Lamoureux, 2019) and according 2D atmospheric background profiles. The modelling shows, as expected from the effective sound speed ratio, a suitable stratospheric duct and rays bouncing between the ground and the middle atmosphere. In all 7 cases, we see a stratospheric shadow zone to distances up to 120-150 km distance with an occasional second shadow zone at twice this distance. However, for the relevant distance of IS26 beyond 300 km in all of the demonstrated cases an eigenray exists between source and receiver.

Lastly, while gravity wave perturbation have proven to be effective in explaining detections within shadow zones, because the fine structure introduced within the stratospheric model often enables eigenrays to reach recording stations that are otherwise missed (e.g. Pilger et al., 2013), we have not seen the opposite case. This can be explained by the tendency of this approach not necessarily to shift a shadow zone, but rather to narrow it, so that stations close to shadow zone boundaries are reached by eigenrays. A similar argument can also be made for the case of parabolic equation modelling (Waxler et al., 2017b), with its ability to illuminate regions, for which ray tracing cannot provide adequate eigenrays.

6. Discussion and conclusions

Over two decades, or annual seasons, a repeatable infrasound ground truth source, providing a consistent and controlled environment compared to the case of other sources of infrasound such as rocket launches (Pilger et al., 2021) or accidental explosions (cf. Campus, 2004; Campus & Christie, 2010) has been observed by IMS station IS26 at a regional distance of about 320 km. Within this distance stratospheric wave propagation develops including the occurrence of acoustic shadow zones. This phenomenon has therefore been observed over a larger range of atmospheric states and is clearly reflected by the two main seasons, summer and winter, being divided by the spring and fall equinoxes.

With the large number of 159 test events we have studied here our ability of detecting infrasound signals from the ground truth source and how it correlates with the development of a stratospheric duct. This duct is consistently absent for the path considered, from west-northwest to east-southeast, for the summer months, as reflected by a fairly stable effective sound speed ratio below 0.9. During equinox times this ratio changes regularly in time to values above 0.95 and mostly above 1.0 enabling stratospheric wave propagation. However, in winter months the effective sound speed ratio is highly variable reaching values up to 1.4-1.5. Even though stratospheric ducting is thus given in principle, it does not necessarily lead to waves that reach an infrasound station, if it is located in a shadow zone.

Therefore, of the nearly 90 cases with suitable atmospheric states to observe a stratospheric arrival, we find 20 cases without signal detection at IS26. While two thirds of these cases can be attributed to the occurrence of an acoustic shadow zone, we find a substantial portion, where the atmospheric model fails to produce a shadow zone and therefore failing to explain the arrival. In these cases, however, we do not observe increased levels of background noise.

In general, for the 71 detections out of the 159 tests we note that at least 25 observations were made for cases with the ECMWF model showing a shadow zone. With the previous finding we can hypothesize that for regional infrasound propagation we should expect in about 30% of cases that the modeling will not be able to explain the signal at hand, if it is expected to have a stratospheric propagation path. Such a finding is supported by recent studies of Fuchs et al. (2019) and Koch & Pilger (2020) for an explosion source in the same general area of Central Europe, where strong evidence for stratospheric arrivals was found, but propagation modeling failed to support these findings.

Acknowledgements and Data Availability Statement

This research was carried out within the German National Data Centre activities based on its mandate towards verification of the Comprehensive Nuclear-Test-Ban Treaty (CTBT). Atmospheric model data were retrieved from the European Centre for Medium-Range Weather Forecasts (ECMWF), see www.ecmwf.int. The infrasound data of IS26 are available from the BGR archive at the International Federation of Digital Seismograph Networks (FDSN) data centers, accessible via www.fdsn.org/datacenters/.

References

Blanc, E. et al., 2018. Toward an improved representation of middle atmospheric dynamics thanks to the ARISE project, Surv. Geophys., 39, 171–225.

Campus, P. (2004). The IMS infrasound network and its potential for detection of events: examples of a variety of signals recorded around the world, InfraMatics, 6, 13-22.

Campus, P. and D. Christie (2010), Worldwide observations of infrasonic waves, in: Le Pichon, A., E. Blanc, and A. Hauchecorne (Eds.), Infrasound Monitoring for Atmospheric Studies, Springer, Heidelberg, Germany. ISBN: 978-1-4020-9507-8, p.185-234.

Dahlman, O., S. Mykkeltveit & H. Haak (2009). Nuclear test ban: converting political visions to reality, Springer Netherlands, pp. 250, ISBN: 978-1-4020-6883-6, doi: 10.1007/978-1-4020-6885-0.

Drob, D.P., J.T. Emmert, J.W. Meriwether, J.J. Makela, E. Doornbos, M. Conde, G. Hernandez, J. Noto, K.A. Zawdie, S.E. McDonald, J.D. Huba, J.H. Klenzing (2015). An update to the Horizontal Wind Model (HWM): the quiet time thermosphere, Earth and Space Science, 2, 301-319, doi: 10.1002/2014EA000089.

Fuchs, F., F. M. Schneider, P. Kolinsky, S. Serafin & G. Bokelmann(2019). Rich observations of local and regional infrasound phases made by the AlpArray seismic network after refinery explosion. Scientific Reports, 9, 13027, doi: 10.1038/s41598-019-49494-2.

Gardner, C.S., C.A. Hostetler& S.J. Franke (1993). Gravity wave models for the horizontal wave number spectra of atmospheric velocity and density fluctuations, J. Geophys. Res., 98, 1035-1049, doi: 10.1029/92JD02051.

Gibbons, S.J., V. Asming, L. Eliasson, A. Fedorov, J. Fyen, J. Kero, E. Kozlovskaya, T. Kværna, L. Liszka, S.P. Näsholm, T. Raita, M. Roth, Y. Vinogradov (2015). The European Arctic: a laboratory for seismoacoustic studies, Seism. Res. Lett., 86, 917–928, doi: 10.1785/0220140230.

Green, D.N., J. Vergoz, R. Gibson, A. Le Pichon & L. Ceranna (2011). Infrasound radiated by the Gerdec and Chelopechene explosions: propagation along unexpected paths, Geophys. J. Int., 185, 890–910, doi: 10.1111/j.1365-246X.2011.04975.x.

Gutenberg, B. (1939). The velocity of sound waves and the temperature in the stratosphere in Southern California, Bull. Amer. Met. Soc., 20, 192-201.

391 Hupe, P., L. Ceranna, C. Pilger, M. de Carlo, A. Le Pichon, B. Kaifler& M. Rapp (2019). Assessing the
392 middle atmosphere weather models using infrasound detections from microbaroms, Geophys. J. Int.,
393 216, 1761-1767, doi: 19.1093/gji/ggy520.

394 Koch, K. (2010). Analysis of signals from an unique ground-truth infrasound source observed at IMS
395 station IS26 in Southern Germany, Pure Appl. Geophys., 167, 401-412.

396 Koch, K. & C. Pilger (2019). Infrasound observations from the site of past underground nuclear
397 explosions in North Korea, Geophys. J. Int., 216, 182–200, doi: 10.1093/gji/ggy381.

398 Koch, K. & C. Pilger (2020). A comprehensive study of infrasound signals detected from the Ingolstadt,
399 Germany, explosion of 1 September 2018, Pure Appl. Geophys., 177, 4229, doi: 10.1007/s00024-020-
400 02442-y

401 Le Pichon, A., J. Vergoz, P.Herry & L. Ceranna (2008). Analyzing the detection capability of infrasound
402 arrays in Central Europe, J. Geophys. Res. 113, D12115.

403 Le Pichon, A., L. Ceranna & J. Vergoz (2012). Incorporating numerical modeling into estimates of the
404 detection capability of the IMS infrasound network, J. Geophys. Res., 117, D05121, doi:
405 10.1029/2011JD016670.

406 Le Pichon,A., J.D. Assink, P. Heinrich,E. Blanc, A. Charlton-Perez, C. F. Lee, P. Keckhut, A. Hauchecorne,
407 R. Rüfenacht, N. Kämpfer, D. P. Drob, P. S. M. Smets, L. G. Evers, L. Ceranna, C. Pilger, O. Ross & C.
408 Claud (2015). Comparison of co-located independent ground-based middle atmospheric wind and
409 temperature measurements with numerical weather prediction models, J. Geophys. Res. Atmos., 120,
410 8318–8331, doi: 10.1002/2015JD023273.

411 Margrave, G.F. & M.P. Lamoureux (2019). Numerical methods of exploration seismology - with
412 algorithms in MATLAB®, Cambridge University Press, ISBN: 9781316756041, doi:
413 10.1017/9781316756041.

414 Negraru, P. T., P. Golden & E. T. Herrin (2010). Infrasound propagation in the ”Zone of Silence”,
415 Seismol. Res. Lett., 81, 614-624, doi: 10.1785/gssrl.81.4.614.

416 Picone, J. M., A. E. Hedin, D. P. Drob& A. C. Aikin (2002). NRLMSISE-00 empirical model of the
417 atmosphere: statistical comparisons and scientific issues, J. Geophys. Res., 107 (A12), 1468, doi:
418 10.1029/2002JA009430.

Pilger, C., F. Streicher, L. Ceranna & K. Koch (2013). Application of propagation modeling to verify and discriminate ground-truth infrasound signals at regional distances, Inframatics, 2, 39-55, doi: 10.4236/inframatics.2013.24004.

Pilger, C., L. Ceranna, J. O. Ross, J. Vergoz, A. Le Pichon, N. Brachet, E. Blanc, J. Kero, L. Liszka, S. Gibbons, T. Kvaerna, S.P. Näsholm, E. Marchetti, M. Ripepe, P. Smets, L. Evers, D. Ghica, C. Ionescu, T. Sindelarova, Y. Ben Horin & P. Mialle(2018). The European Infrasound Bulletin, Pure Appl.Geophys., 175, 3619–3638, doi:10.1007/s00024-018-1900-3.

Pilger, C., P. Hupe, P. Gaebler & L. Ceranna (2021). 1001 rocket launches for space missions and their infrasonic signature, Geophys. Res. Lett., 48, e2020GL092262, doi: 10.1029/2020GL092262

Stammler, K. (1993). SeismicHandler—Programmable multichannel data handler for interactive and automatic processing of seismological analyses, Computers and Geosci. 19, 135–140.

Sutherland, L. C & H.E. Bass (2004). Atmospheric absorption in the atmosphere up to 160 km, J. Acoust. Soc. Am. 115, 1012–1032, doi: 10.1121/1.1631937.

Waxler, R., J. Assink & D. Velea (2017a). Modal expansions for infrasound propagation and their implications for ground-to-ground propagation, J. Acoust. Soc. Am. 141, 1290–1307, doi: 10.1121/1.4976067.

Waxler, R., J. Assink, C. Hetzer & D. Velea (2017b). NCPAprop—A software package for infrasound propagation modeling. J. Acoust. Soc. Am., 141, 3627, doi: 10.1121/1.4987797.

439 Table 1: Monthly statistics of the numbers of ARIANE engine tests detected or non-detected in the
440 years 2000-2019, also giving the portion in each category. Note the total or nearly total lack of
441 detections in May-September, or summer months, while the majority of engine test from October-
442 April, or winter months, are observed.

443

Month	Det.		Non-Det.		Total
Jan	9	(69%)	4	(31%)	13
Feb	8	(73%)	3	(27%)	11
Mar	13	(76%)	4	(24%)	17
Apr	10	(56%)	8	(44%)	18
May	1	(8%)	12	(92%)	13
Jun	0	-	11	(100%)	11
Jul	0	-	21	(100%)	21
Aug	0	-	14	(100%)	14
Sep	1	(17%)	5	(83%)	6
Oct	8	(73%)	3	(27%)	11
Nov	10	(91%)	1	(9%)	11
Dec	11	(85%)	2	(15%)	13
Sum	71		88		159

444
445

446

Table 2: Detection statistics compared to effective sound speed ratio and stratospheric shadow zone. In each cell the first number is the count for those propagation models that show a stratospherically ducted path to IS26, while the second number gives the counts with a shadow zone. An asterisk indicates a case where the shadow zone is questionable (see also footnotes). For example, in the second column ($1.1<v_{eff\text{-}ratio}<1.2$) there are 9 good signal detections with a stratospheric path to the station, and one good detection, where the station is possibly within a shadow zone. Note: Of the 71 observed signal detections 41 are predicted/confirmed by the ECMWF model with varying signal levels, while for 30 cases the station is predicted to be, or possibly be, within a shadow zone (see marked cells in "Row sum" column). With the benefit of doubt for the 5 cases of uncertainty (potentially resolved by using gravity wave perturbations) 46 explained cases are offset by 25 unexplained/shadow zone cases. Furthermore, there are 7 non-detections when the $v_{eff\text{-}ratio}$ is distinctly above 1, but not any associated shadow zone. For further discussion of the 20 non-detection cases within the framed cells, refer to Table 3.

	$v_{eff\text{-}ratio}>1.2$	$1.1<v_{eff\text{-}ratio}<1.2$	$1<v_{eff\text{-}ratio}<1.1$	$0.98<v_{eff\text{-}ratio}<1$	$v_{eff\text{-}ratio}<0.98$	Row sum
Detection(2)	**25** / 0	**9** / 1*	**0** / 2	-	-	**34** / 3*
Detection(1)	**4** / 0	**1** / 6*	**0** / 4*	- / 3	-	**5** / 13^{2*}
Detection(0)	**0** / 2*	**1** / 5	**1** / 6*	- / 1	-	**2** / 14^{2*}
Non-detection	4 / **1**	3 / **6***	0 / **6***	- / **9***	- / **59**	7 / $\mathbf{81}^{3*}$
Column total [# incon'cies]¥	36 [5]	32 [13]	19 [10]	13 [4]	59	159 [32]

*) 1 stratospheric shadow zone is questionable

^{2*}) 2 stratospheric shadow zones are questionable

^{3*}) 3 stratospheric shadow zones are questionable

¥) Number of inconsistencies, i.e. the underlined numbers above, but neglecting the cases of questionable shadow zones (marked by asterisks)

Table 3: List of ARIANE engine tests for which a stratospheric duct exists based on the atmospheric model (ECMWF) ($v_{eff\text{-}ratio}$>1), but for which no signals could be identified at IS26. The highlighted entries (bold text) indicate those tests, where the propagation modeling does not produce a shadow zone at or near IS26, while for other entries such a shadow zone exists (even if doubtful, as indicated by a question mark).

Test [ID #]	Date [YYYY MM DD HH]	Shadow Zone	Effective Sound Speed Ratio
150	**2015 12 10 11**	**N**	**1.298**
004	**2000 03 09 15**	**N**	**1.227**
062	**2002 03 15 14**	**N**	**1.225**
058	2002 01 31 14	Y	1.218
172	**2019 02 21 14**	**N**	**1.208**
106	2006 11 14 13	Y	1.192
170	2019 01 17 14	Y	1.184
157	**2018 01 22 12**	**N**	**1.152**
052	2001 10 25 13	Y	1.148
029	**2000 12 07 15**	**N**	**1.146**
002	**2000 01 21 16**	**N**	**1.141**
173	2019 03 07 15	Y	1.124
064	2002 04 04 13	?	1.104
115	2009 10 14 14	Y	1.103
023	2000 10 09 14	Y	1.097
066	2002 04 26 14	Y	1.057
037	2001 04 05 13	Y	1.050
088	2004 04 16 13	Y	1.048
146	2015 09 28 13	Y	1.047
041	2001 05 04 12	?	1.007

Figures:

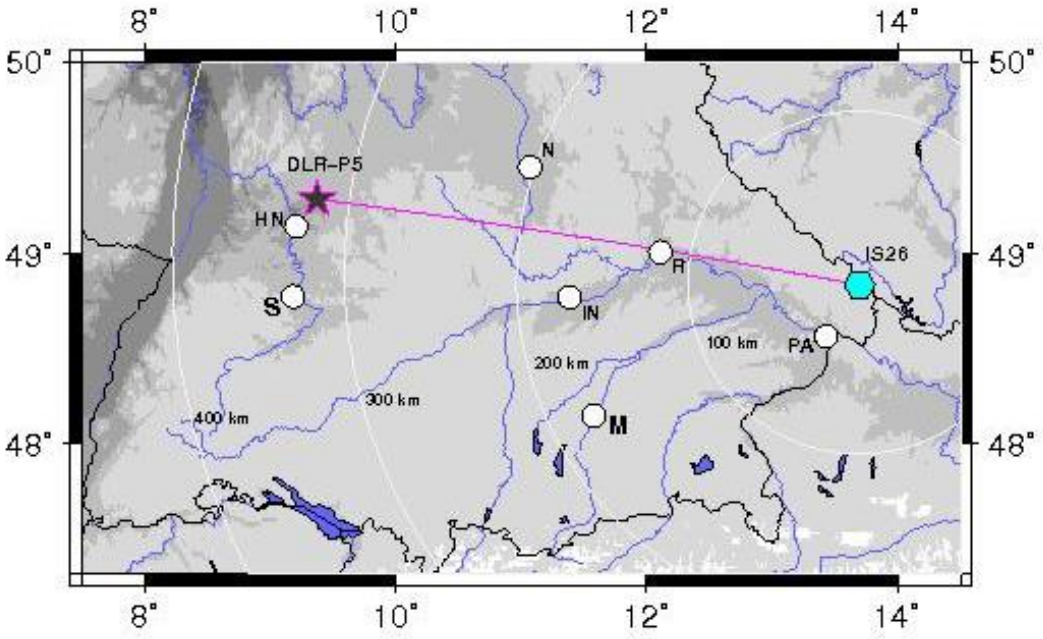

Fig.1: Geographical map showing the location of the propulsion test facility P5 of DLR (star) near Heilbronn (denoted by HN label) and the IMS infrasound station IS26 (hexagon) in the Bavarian forest. Distance circles in increments of 100km are also displayed, with IS26 at a range of 320 km and with a backazimuth of 280° from the P5. Additionally, the locations of major cities in southern German are given: Stuttgart (S), Nuremberg (N), Ingolstadt (IN), Munich (M), Regensburg (R), and Passau (PA).

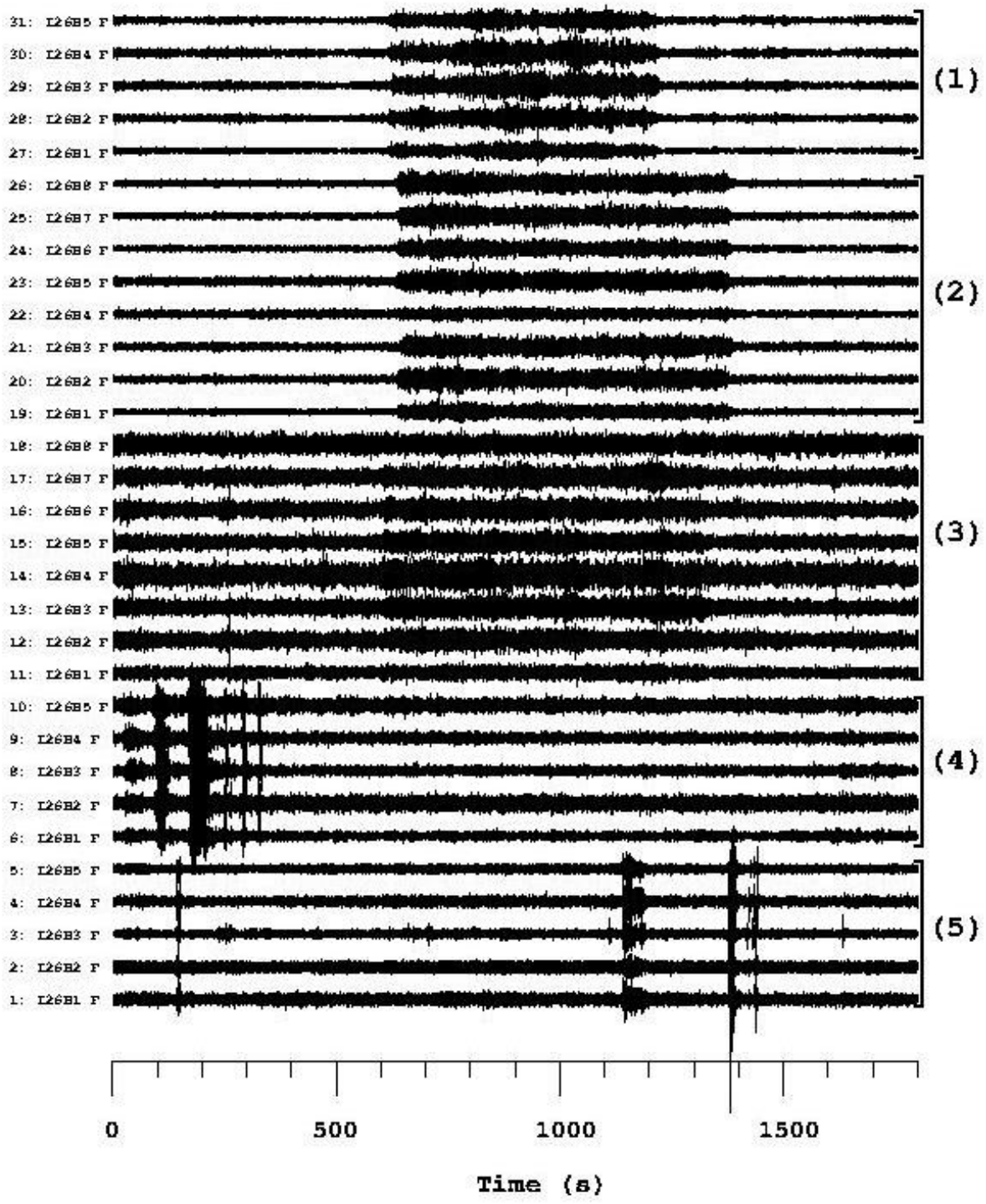

Fig.2: Waveform recordings of infrasound signals at IS26 for 5 ARIANE engine tests showing good signals for the top two events, fair to poor signals for the middle event, and no signals for the two bottom events (from top to bottom: (1) 23-Nov-2000, (2) 14-Feb-2013, (3) 16-Feb-2012, (4) 7-Dec-2000, (5) 3-Jul-2001). All engine tests had durations of more than 600 s, as can be deduced from the traces for the top three events.

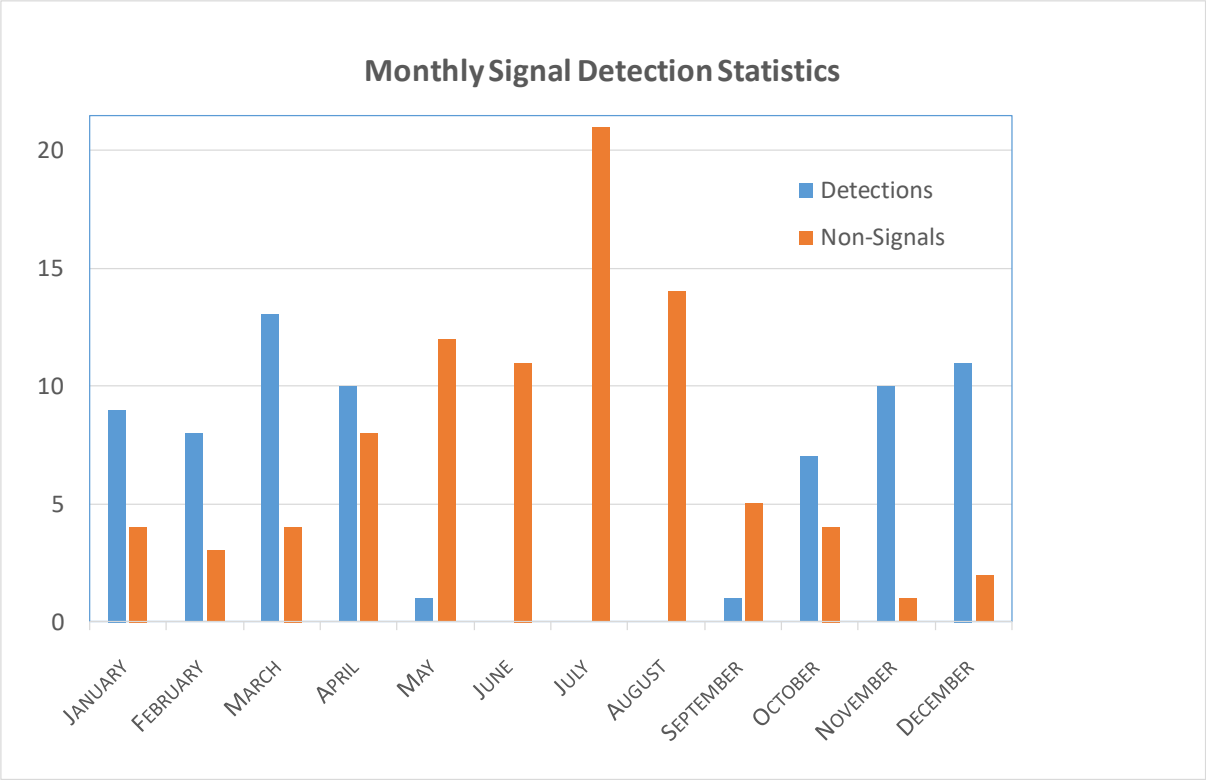

489

490 Fig.3: Monthly statistics on signal observations/detections and non-detections for the years 2000-
491 2019, with the 70 detections being distributed almost exclusively between October and April (and not
492 detections in Jun-Aug), while non-detections being mainly observed in summer, but rarely also during
493 winter months.

494

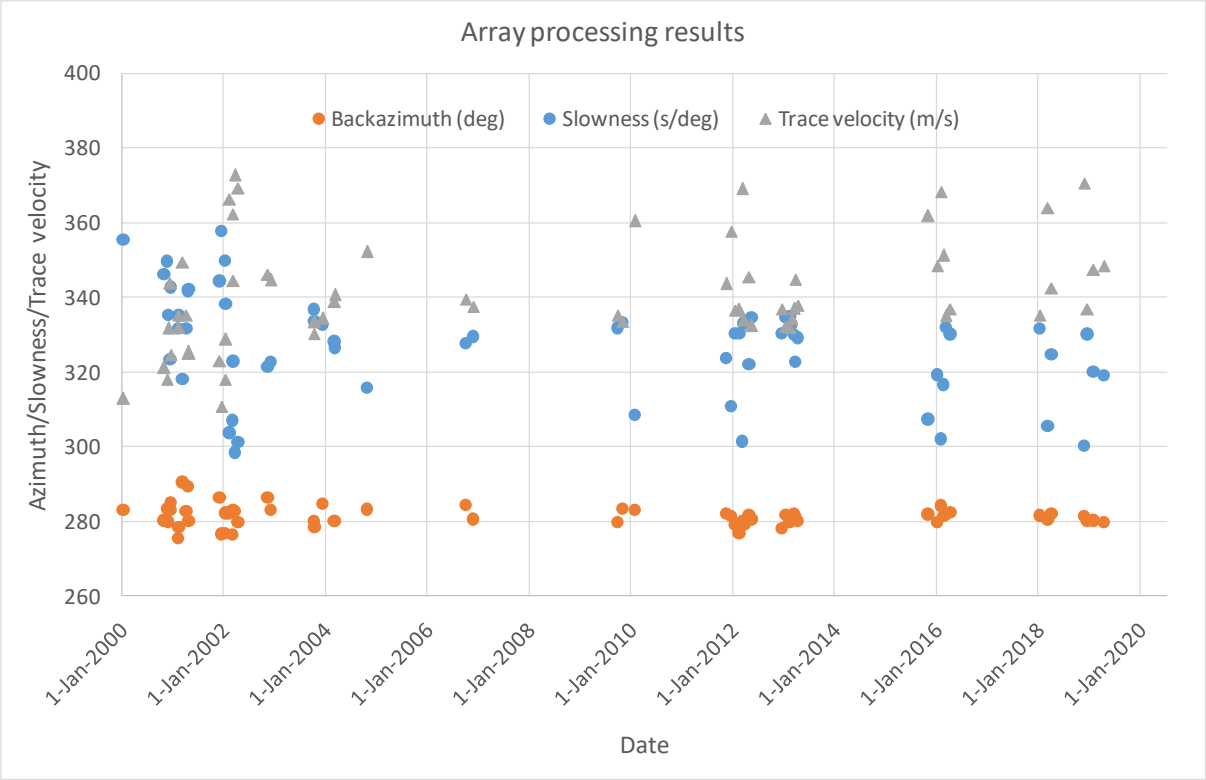

495

496 Fig.4: Results of the array data processing for the infrasound signals at IS26. The backazimuth scatters
497 around the theoretical value by about ±5° The slowness estimate from FK analysis (i.e. output of the
498 applied software) converted to apparent (or trace) velocity scatters between 310 and 370 m/s. Note
499 the larger uncertainties before 2008, which may be related to the smaller number of five array
500 elements compared to the present-day eight elements.

501

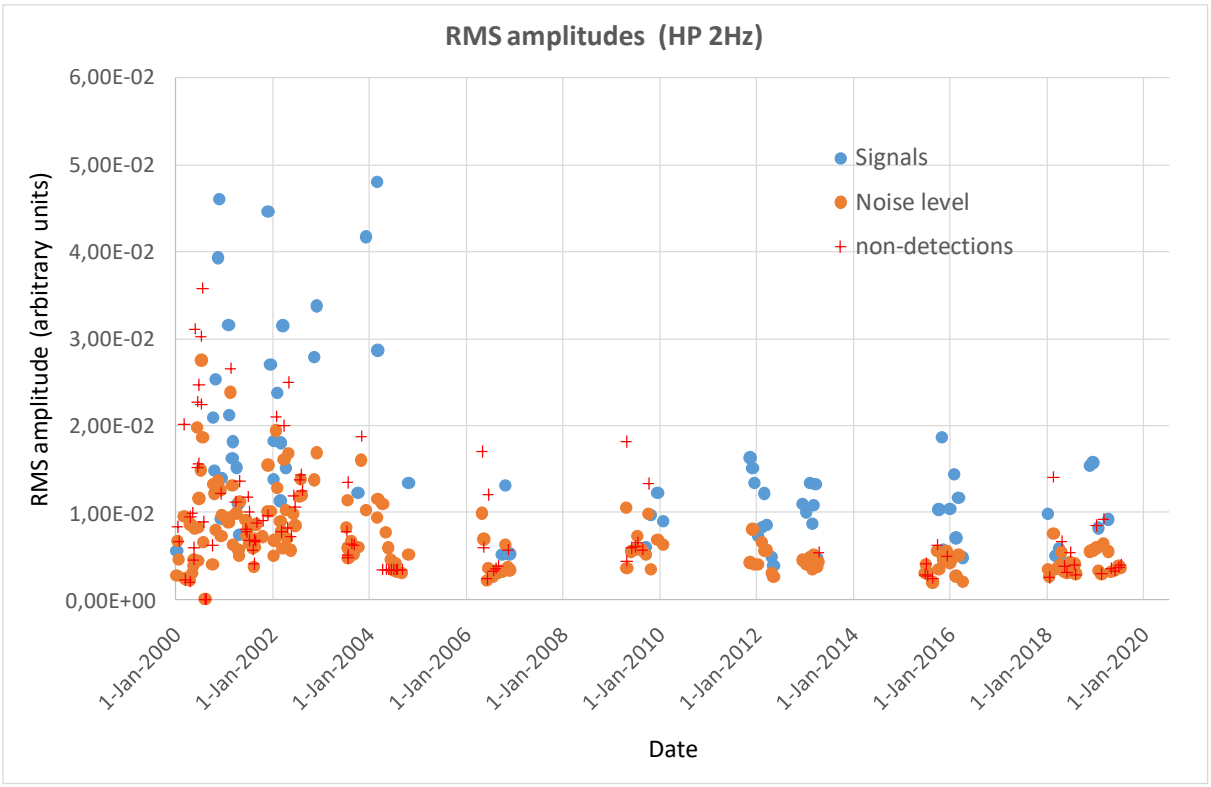

502

503 Fig.5: RMS amplitude measurements for signals (blue dots) and pre-signal noise levels (orange dots) for
504 detection and noise levels for non-detections (red- crosses). Note the larger scatter prior to the year
505 2004 propagation when impedance filters were installed at the infrasound station.

506

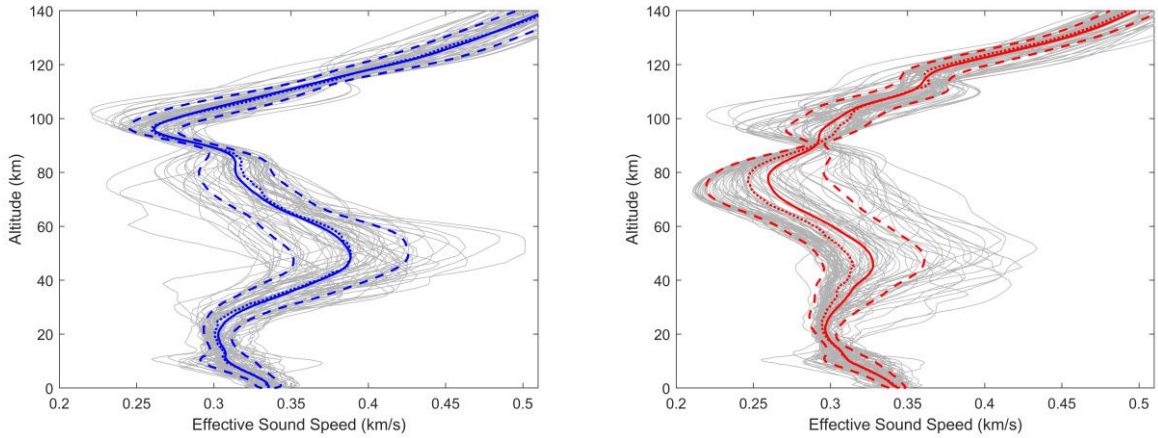

507

508 Fig.6: Effective sound speed profiles from the surface to an altitude of 140 km based on ECMWF
509 models for time s of (a - left) signal detections, and (b - right) non-detections. From the individual
510 models (gray lines) a mean (solid line) and median model (dotted line) was determined, as well as the
511 associated standard deviations (dashed lines). For case (a) the mean and median models are nearly
512 identical, while in the case of non-detections they are significantly different.

513

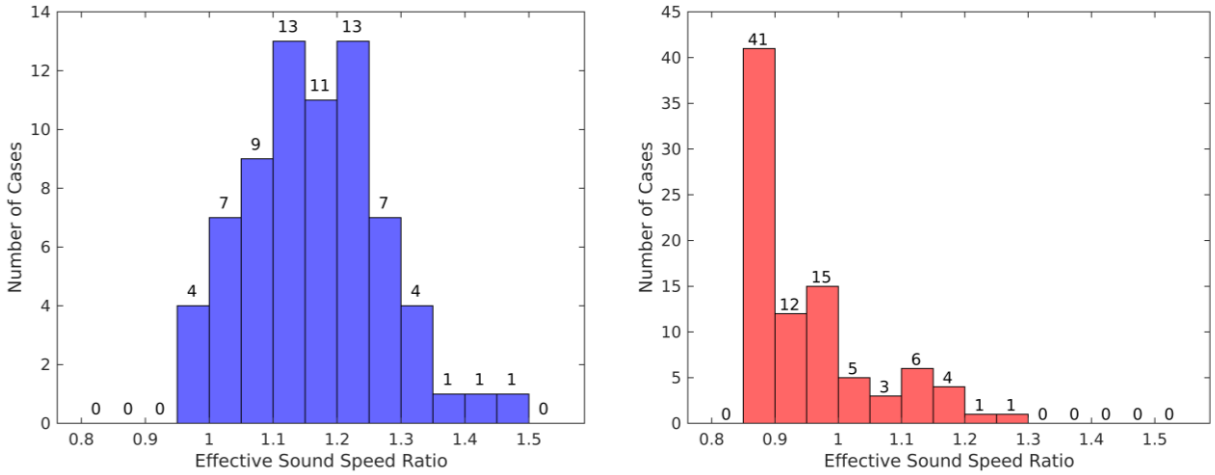

514

515 Fig.7: Histograms of the effective sound speed ratio of the ECMWF models for the cases with signal
516 detections from ARIANE engines tests (a-left) and for cases for which no signals could be found (b-
517 right). For signal detections, the $v_{eff\text{-}ratio}$ of the ECMWF models is larger than 1 except for four cases.
518 For nearly half of tests it is between 0.85 and 0.9, but in 20 cases the $v_{eff\text{-}ratio}$ exceeds 1.0, indicative
519 for the existence of a stratospheric duct.

520

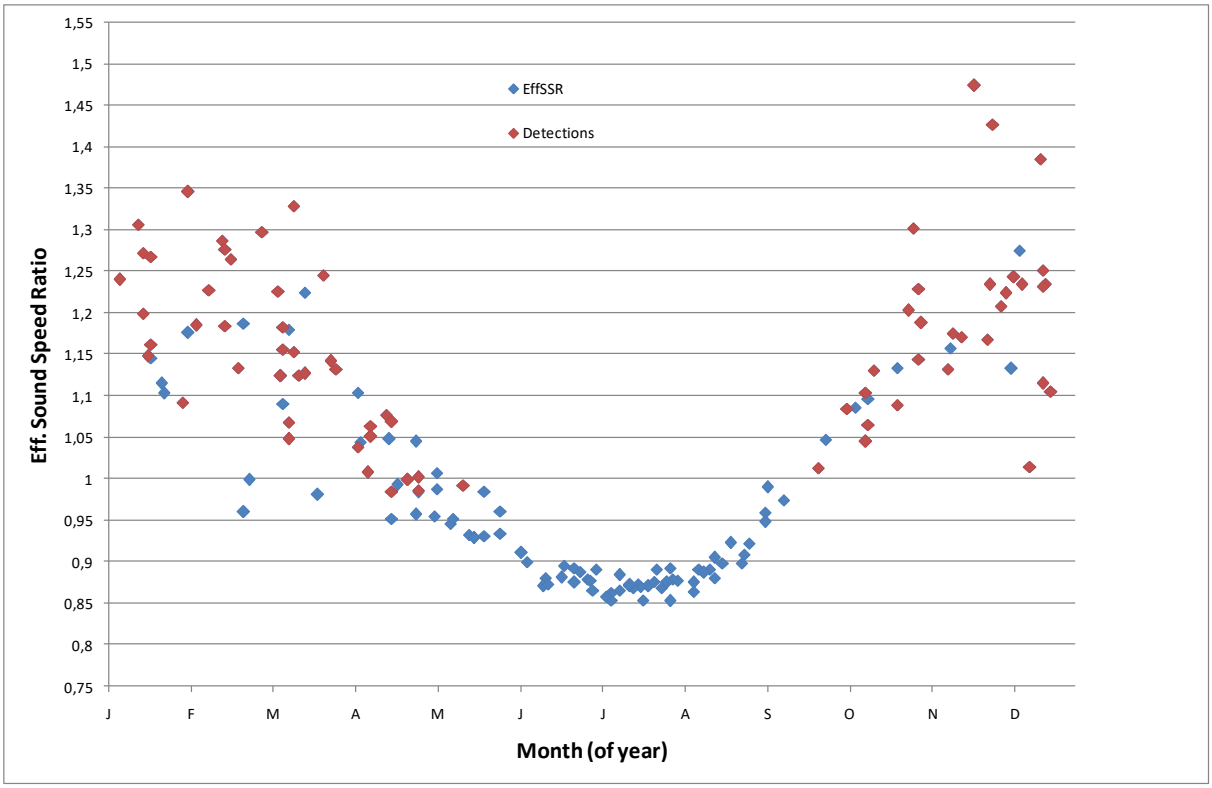

Fig.8: The effective sound speed ratios for the atmospheric models associated with the 71 signals detections and 88 non-detections. Cases with signal detections are marked with red symbols, while cases with non-detections are shown in blue. For the summer months June through August the $v_{eff\text{-}ratio}$ is fairly stable between 0.85 and 0.9 and associated with the lack of any detection. For the remained of the year, both detections and non-detections can occur.

A) case150

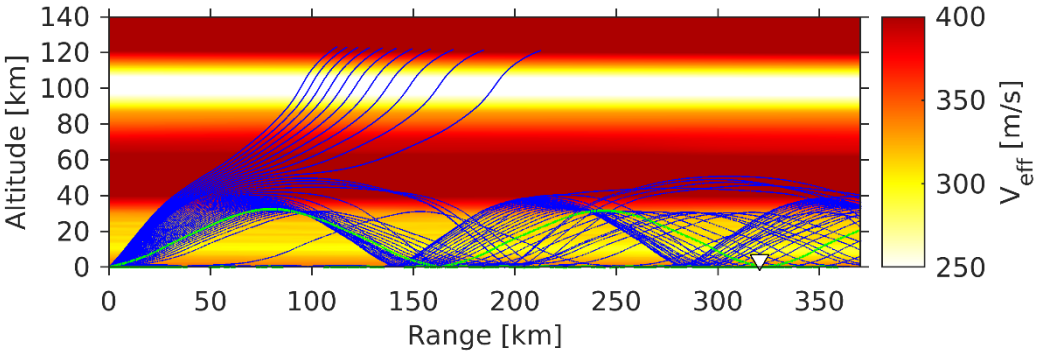

B) case004

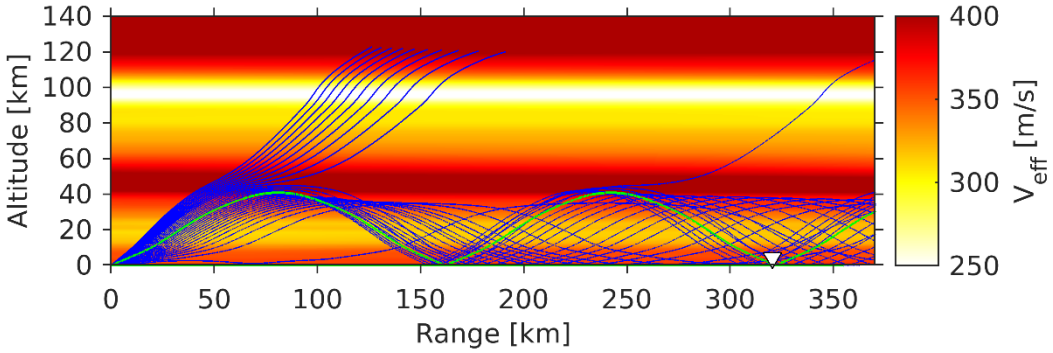

C) case062

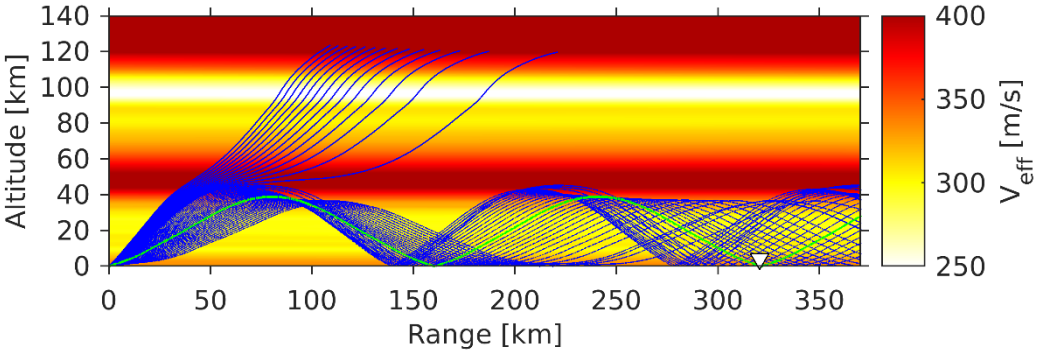

D) case172

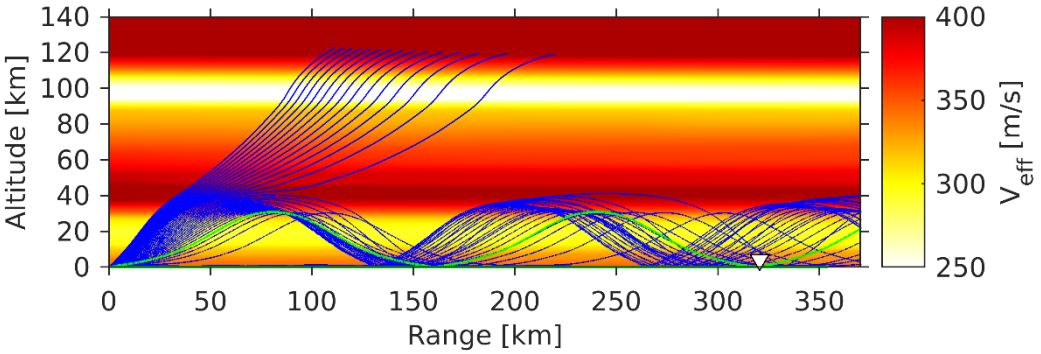

Fig.9 (cont'd)

E) case157

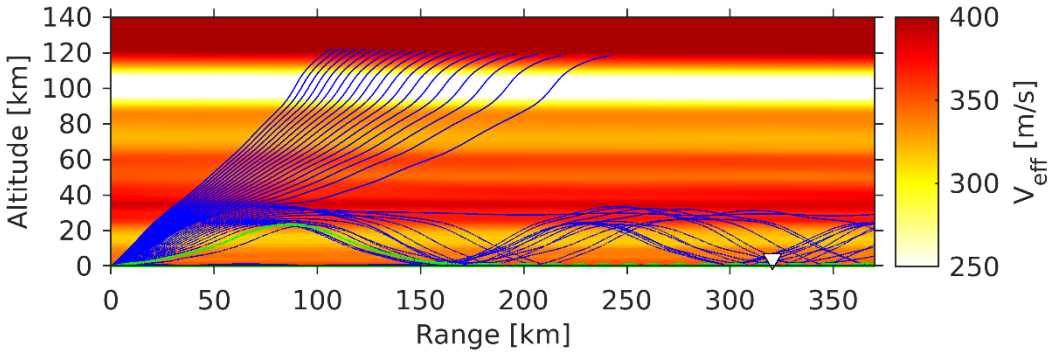

F) case029

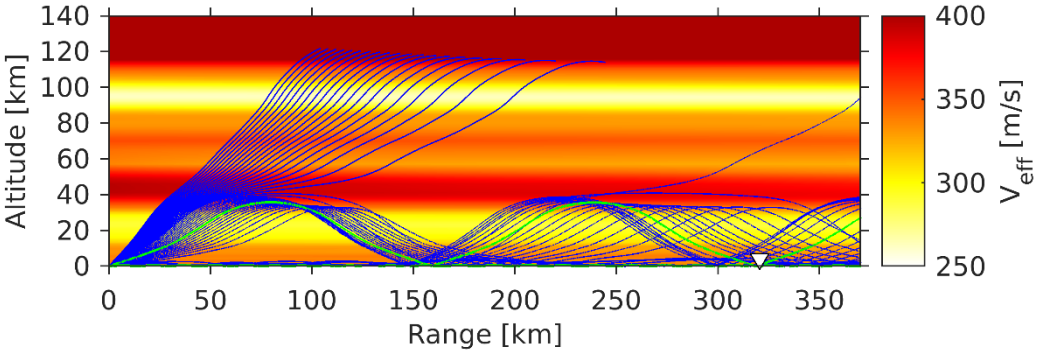

G) case 002

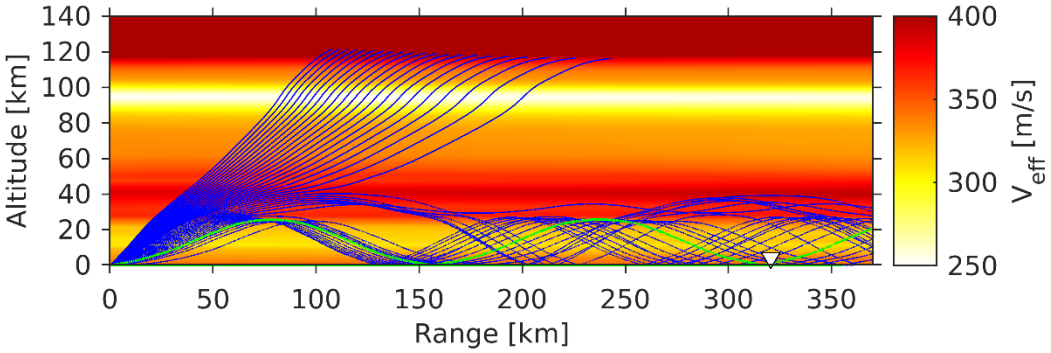

Fig.9: Two-dimensional ray-trace propagation modeling between the DLR rocket engine test facility (axes origin) and infrasound array IS26 (white triangle) for the 7 non-detection cases. ECMWF models provide effective sound speed values (V_{eff}, color-coded) being larger than the effective sound speed near the ground (thus effective sound speed ratio >1), showing a suitable stratospheric duct without a shadow zone near the station.

Figure 1.

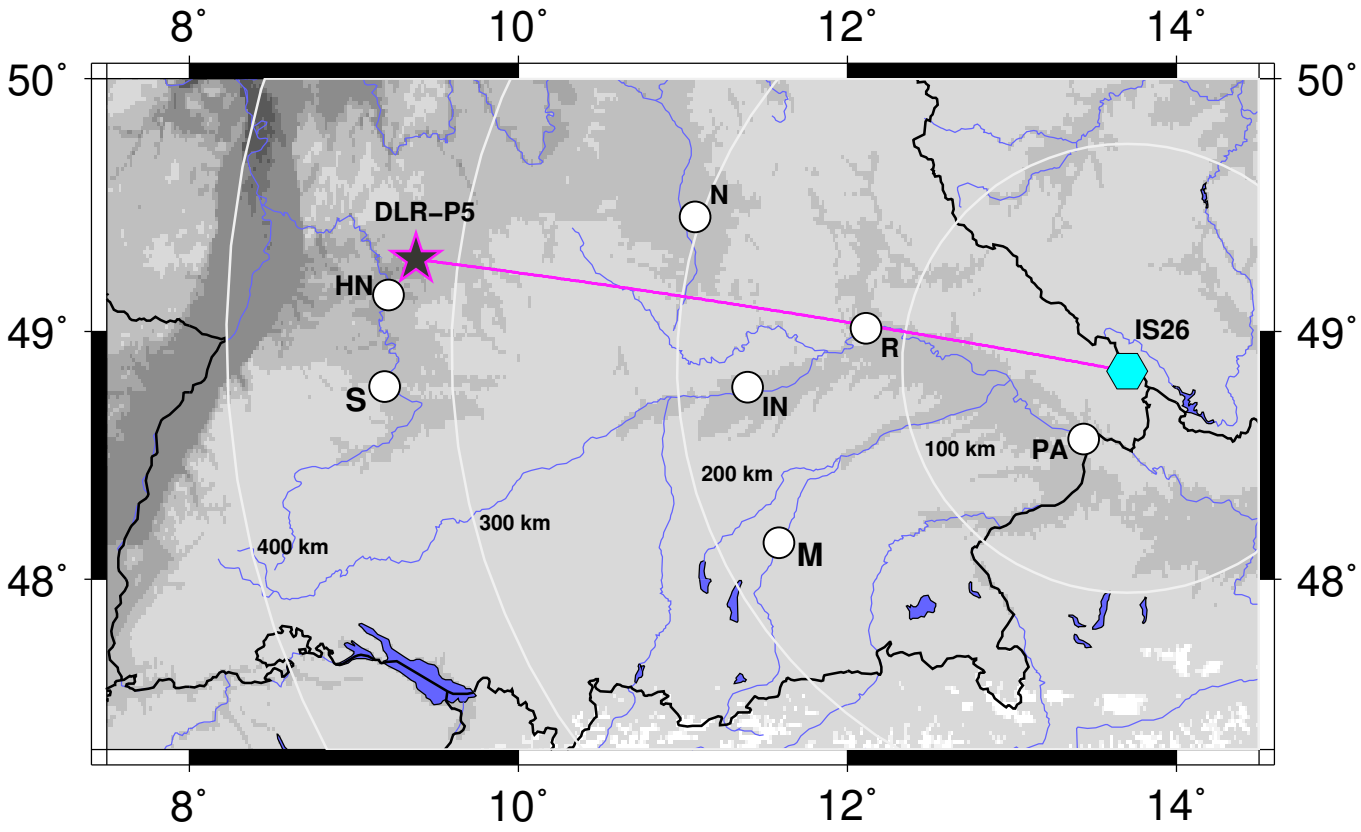
8˚
10˚
12˚
14˚
50˚
49˚
48˚
DLR–P5
HN
N
R
IS26
S
IN
PA
M
100 km
200 km
300 km
400 km

Figure 2 (small version).

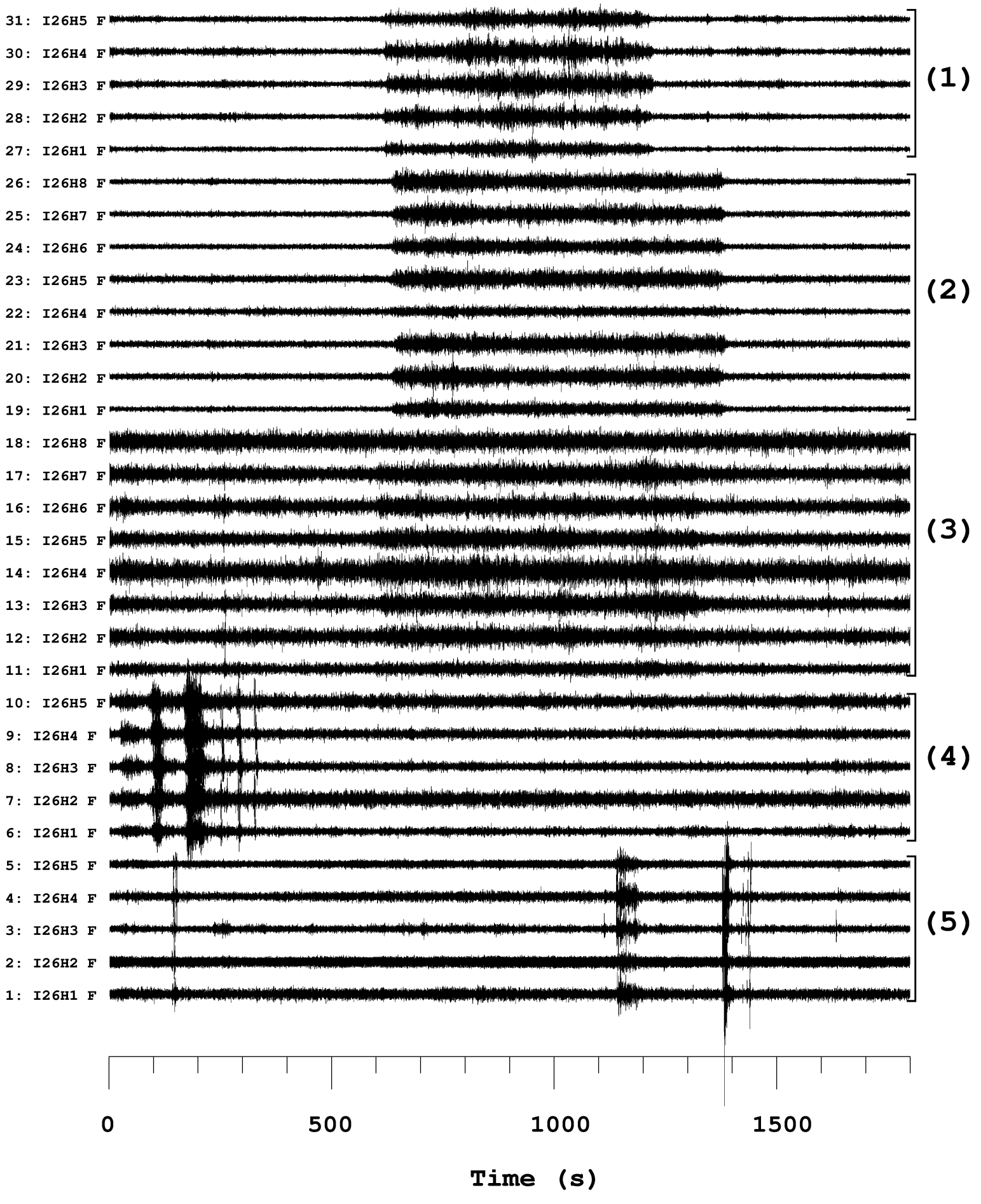
31: I26H5 F
30: I26H4 F
29: I26H3 F
28: I26H2 F
27: I26H1 F
26: I26H8 F
25: I26H7 F
24: I26H6 F
23: I26H5 F
22: I26H4 F
21: I26H3 F
20: I26H2 F
19: I26H1 F
18: I26H8 F
17: I26H7 F
16: I26H6 F
15: I26H5 F
14: I26H4 F
13: I26H3 F
12: I26H2 F
11: I26H1 F
10: I26H5 F
9: I26H4 F
8: I26H3 F
7: I26H2 F
6: I26H1 F
5: I26H5 F
4: I26H4 F
3: I26H3 F
2: I26H2 F
1: I26H1 F
(1)
(2)
(3)
(4)
(5)
0
500
1000
1500
Time (s)